Evolution of Carbon Nanofiber-Supported Pt Nanoparticles of Different Particle Sizes: A Molecular Dynamics Study

Hongye Cheng,[a] Yi-An Zhu,[a,*] De Chen,[b] Per-Olof Åstrand,[c] Ping Li,[a] Zhiwen Qi,[a] and Xing-Gui Zhou[a]

[a]State Key Laboratory of Chemical Engineering, East China University of Science and Technology, Shanghai 200237, China

[b]Department of Chemical Engineering and [c]Department of Chemistry, Norwegian University of Science and Technology (NTNU), 7491 Trondheim, Norway

Corresponding Author:

*E-mail: yanzhu@ecust.edu.cn

*Tel: +86 21 6425 3072

Abstract: Molecular dynamics simulations based on a bond-order force field (ReaxFF) have been performed to examine the structural evolution of fishbone-type carbon nanofiber-supported Pt nanoparticles, with particle size ranging from 5.6 Å to 30.7 Å. Calculated results indicate that upon adsorption the distribution of first-shell Pt-Pt coordination number and radial distribution function change significantly in Pt nanoparticles up to 2 nm in size, and the restructuring degree of the Pt nanoparticles decreases with particle size, which is attributed both to the reduced binding energy per Pt atom bonded to the support and to the increased cohesive energy of the Pt nanoparticles. In the Pt_{10} particle, the majority of the Pt atoms are detached from the metal particle, leading to atomic adsorption of single Pt atoms on the support. As the Pt particle size is increased to ~3 nm, however, the crystalline degree of Pt nanoparticles is even higher than that of the corresponding isolated ones because the strong metal-support interaction has a positive effect on the crystalline degree of the upper part of Pt nanoparticles. Two surface properties of the Pt nanoparticles, namely, Pt dispersion and surface first-shell Pt-Pt coordination number, are then computed and found to decrease and increase, respectively, with particle size. Thus, on-purpose control of particle size (and hence the metal-metal and metal-support interaction) is of crucial importance to tune the superficial structures of supported active metal particles, which eventually determine the adsorption and catalytic properties of catalysts.

Keywords: Supported Pt catalyst, ReaxFF, Cohesive energy, PEMFC, Shape-control

1. INTRODUCTION

Size-dependent catalytic properties of supported metal nanoparticles have been the subject of extensive investigations.[1-6] The dispersion of metal atoms in catalysts is approximately equal to the reciprocal of metal particle size in nanometers;[7,8] that is, small metal particles have more atoms or active sites exposed than large ones provided that the metal loading is identical, which in turn gives rise to a higher catalytic efficiency for structure-insensitive reactions. On the other hand, metal nanoparticles can be viewed as surrounded by surfaces with different local geometries, such as terraces, steps, kinks, and corners, etc. The sites on these surfaces are distinguished by the number of their nearest neighbors. Small metal particles have much more under-coordinated sites while large ones are dominated by coordinatively saturated terrace sites. Thus, the dependence of catalytic properties of metal nanoparticles on their particle sizes arises from the distinctive adsorption behaviors of different surface sites, which is usually represented in terms of ligand (electronic) and ensemble (structural) effects.[1]

Carbon-supported Pt-based catalyst is among the most attractive materials as electrodes in fuel cells, which exhibits high catalytic activities for both hydrogen/methanol oxidation[9,10] and oxygen reduction reaction (ORR)[11] at low temperature. In particular, Pt particle size was proposed to have a significant effect on the specific activity and mass activity for structure-sensitive methanol oxidation[3,12,13] and ORR.[4,14-21] Frelink et al.[3] found that for the particle size ranging from 1.2 nm to 4.5 nm a reduced particle size results in a decrease in the specific activity for methanol oxidation, while for the particle size greater than 4.5 nm the specific activity keeps almost constant. Shao et al.[4] investigated the ORR in $HClO_4$ solutions with Pt particle size in the range of 1-5 nm. Their results indicated that the specific activity increases rapidly as the particle increases up to 2.2 nm and then slowly with a further increase.

The presence of edge Pt sites which have strong oxygen binding energies was proposed to be the primary reason for the observed low specific activity at low particle sizes. Mayrhofer et al.[18,19] studied the ORR on a carbon-supported Pt catalyst and found that adsorption of oxygenated species is enhanced with decreasing the particle size. The increase in oxophilicity in small particles leads to a decrease in the specific activity for the ORR, because OH_{ad}/O_{ad} can effectively block the active sites required for adsorption of O_2 and/or the splitting of the O-O bond. Nørskov and co-workers[20,21] have demonstrated how the atomic-scale modeling on the surfaces of nanoparticles can assist in understanding particle size effects in electrocatalysis. In their work, density functional theory (DFT) calculations were performed to estimate the ORR kinetics on the Pt(111), Pt(100), and Pt(211) facets.[20] Small particles that have more Pt(211) exhibit lower specific ORR activity than large particles that are dominated by Pt(111) and Pt(100) because O and OH radicals are bound too strongly to the steps and hence increase the energy barrier for water formation at these defect sites.

Since Pt particle size plays a vital role in electrocatalysis, the investigation of the microstructures and properties of supported Pt nanoparticles of different particle sizes is highly desired for rational catalyst design. Carbon nanofibers (CNFs) have many important advantages as an electrode material, including high surface area, inertness in basic and acidic solution,[22] high conductivity,[23,24] and tolerance to CO poisoning.[25] In our previous study regarding Pt_{100} particles supported on fishbone-type CNFs (f-CNFs),[26] four f-CNF cone-helix models with different basal-to-edge surface area ratios and edge plane terminations were employed to represent the surface conditions of carbon supports. Molecular dynamics (MD) simulations based on a reactive force field (ReaxFF) were carried out to examine the interaction between Pt particles and f-CNFs. The calculated results indicated that more exposed f-CNF edge planes

lead to a more negative binding energy of the Pt_{100} particles to the f-CNF and thus to a higher restructuring degree of Pt_{100} particles. As the ReaxFF is well suited to deal with the Pt-CNF system, our early work provides a foundation of studying the evolution of Pt nanoparticles of different particle sizes supported on f-CNFs.

In this contribution, Pt nanoparticles of 10 to 800 atoms are deposited on f-CNF/60, with the particle size ranging from 5.6 Å to 30.7 Å. Their different structural evolution upon adsorption is investigated through MD simulations based on the ReaxFF. As Pt particle size increases, the variations in first-shell Pt-Pt coordination number and radial distribution function in the supported Pt particles are calculated with respect to those in the corresponding isolated Pt particles to quantify the restructuring degree. Pt-C bond length distribution and the binding energies of the Pt particles to the f-CNF are computed to quantitatively represent the Pt-CNF interaction. The cohesive energy of the Pt particles is correlated with their particle size, in order to reveal its negative contribution to Pt particle restructuring. The surface properties of the supported Pt particles, including first-shell Pt-Pt coordination number and Pt dispersion, are finally calculated and the relationship between the microstructures of active metal surfaces and their catalytic properties is elucidated.

2. COMPUTATIONAL DETAILS

2.1. ReaxFF

The ReaxFF is based on a bond-order approach[27,28] and a charge equilibrium scheme[29] parameterized from quantum chemical data, providing a good compromise between accuracy and computational efficiency. The analytical expression of each energy contribution and a detailed explanation of their physical meaning can be found in ref. 30 and the supporting information of ref. 31. The ReaxFF was originally proposed for hydrocarbons[30] and has been

extended to model many systems.[31-37] More recently, it succeeded in accounting for the CNT growth mechanism on Ni.[38-40] In this work, the Pt/C ReaxFF parameters employed were optimized by using DFT calculations with the Perdew-Burke-Ernzerhof (PBE) exchange-correlation functional and norm-conserving pseudopotentials.[41] Early studies have demonstrated the reliability of such Pt/C ReaxFF parameters for depicting the interaction between Pt particle and f-CNF.[26,41,42]

2.2. MD Simulation

MD simulations have been performed using the LAMMPS code[43,44] with the ReaxFF. A time step of 0.25 fs was adopted, which ensures energy conservation of the simulated system through a few trial ReaxFF simulations in the microcanonical ensemble (NVE).[41] The minimization of the system energy was preliminarily conducted before MD simulations. In the MD simulations, we used 50 ps to equilibrate the system at 600 K by using the canonical ensemble (NVT) and the Nosé-Hoover chain thermostat.[45] An MD simulation was subsequently carried out in equilibrium for 250 ps.

2.3 Model Construction

Pt particles containing 10, 20, 50, 100, 150, 200, 300, 400, 500, 600, 700, and 800 atoms (denoted as Pt_{10}, Pt_{20}, Pt_{50}, Pt_{100}, Pt_{150}, Pt_{200}, Pt_{300}, Pt_{400}, Pt_{500}, Pt_{600}, Pt_{700} and Pt_{800} particles, respectively) were constructed on the basis of the fcc structure. Before the Pt particles were supported on f-CNFs, simulated annealing was performed to get stable particle structures. The minimization was combined with 20 cycles of MD simulations from 300 K to 1500K and then back from 1500 K to 300 K. After the annealing simulation, the diameters of Pt particles range from 5.6 Å to 30.7 Å, as listed in Table 1, and the structures of the isolated particles are shown in Figure S1 (see Supporting Information).

Table 1. Structural parameters of Pt/f-CNF models

	Size of isolated Pt particle (Å)	Number of helical cones of f-CNF/60 in one cell	Number of atoms in f-CNF/60 model	Cell parameters (Å)		
				a	*b*	*c*
Pt_{10}	5.6	9	13050	150	150	36.48
Pt_{20}	8.3	9	13050	150	150	36.48
Pt_{50}	11.4	9	13050	150	150	36.48
Pt_{100}	15.4	9	13050	150	150	36.48
Pt_{150}	18.5	9	13050	150	150	36.48
Pt_{200}	19.2	9	13050	150	150	36.48
Pt_{300}	21.8	13	18850	160	160	52.70
Pt_{400}	24.7	13	18850	160	160	52.70
Pt_{500}	25.7	13	18850	160	160	52.70
Pt_{600}	28.3	13	18850	160	160	52.70
Pt_{700}	28.9	14	20300	170	170	56.75
Pt_{800}	30.7	14	20300	170	170	56.75

The cone-helix model for f-CNF was obtained with a continuous graphite ribbon spiraling along the principal axis.[46] The effect of the basal-to-edge surface area ratio of f-CNF on the interaction between f-CNF and Pt_{100} was studied in our previous work.[26] The f-CNF with the disclination angle of 60^o (denoted as f-CNF/60) which has a low basal-to-edge surface area ratio has the greatest interaction with Pt_{100}, and therefore the f-CNF/60 was used in this work to support various Pt particles. The adjacent helical cones of the f-CNF/60 have the same sequence of armchair and zigzag arrangements.[26] The diameter of the f-CNF/60 is increased to 60 Å to eliminate interactions among the three supported Pt particles. Periodic boundary conditions were imposed on the cone-helix models of the f-CNF/60 to depict the f-CNF/60 morphologies along the principal axis. The number of helical cones involved in one cell, the corresponding number of atoms in the f-CNF/60 models, and the cell lengths in the *z* direction are given in Table 1. In order to eliminate the lateral interactions, the cell lengths in the *x* and *y* directions are two times greater than the diameters of the Pt/f-CNF system (see Table 1).

The initial structures of the Pt particles supported on f-CNF/60 are illustrated in Figure S2

(see Supporting Information). The Pt particles were initially placed at a distance of about 2 Å away from the surface sites of f-CNF/60. Three Pt particles were initially placed at an armchair arrangement [denoted as Pt_n(I)], a zigzag arrangement [denoted as Pt_n(II)], and the junction between an armchair and a zigzag arrangement [denoted as Pt_n(III)] of f-CNF/60, where *n* is the number of atoms involved in the Pt particles.

3. RESULTS AND DISCUSSION

3.1 Particle Size Effect on Restructuring Degree of Supported Pt Particles

Schematic representations of the Pt particles (from Pt_{10} to Pt_{800}) adsorbed on the f-CNF/60 after 250 ps of equilibrium are shown in Figure 1. On the basis of the comparison between Figures S2 and 1, all the Pt particles moved more closely to the f-CNF/60 surfaces with the formation of covalent bonds between Pt atoms and the f-CNF/60. The interaction between the Pt particles and f-CNF/60 gives rise to a restructuring of the Pt particles to some extent. The restructuring degree of the Pt particles decreases with the increase in Pt particle size. In small Pt particles (e.g., Pt_{10} shown in Figure 2a), all or most Pt atoms migrate from their initial positions and are adsorbed on the f-CNF surfaces, resulting in a significant restructuring. In large Pt particles (e.g., Pt_{800} shown in Figure 2b), however, only a small fraction of Pt atoms that are located initially at the Pt/f-CNF interfaces are detached from the Pt particles and bonded to the f-CNF, leading to the morphology of particles almost unchanged. Two videos regarding the evolution of the morphologies of Pt particles can be found in Supporting Information.

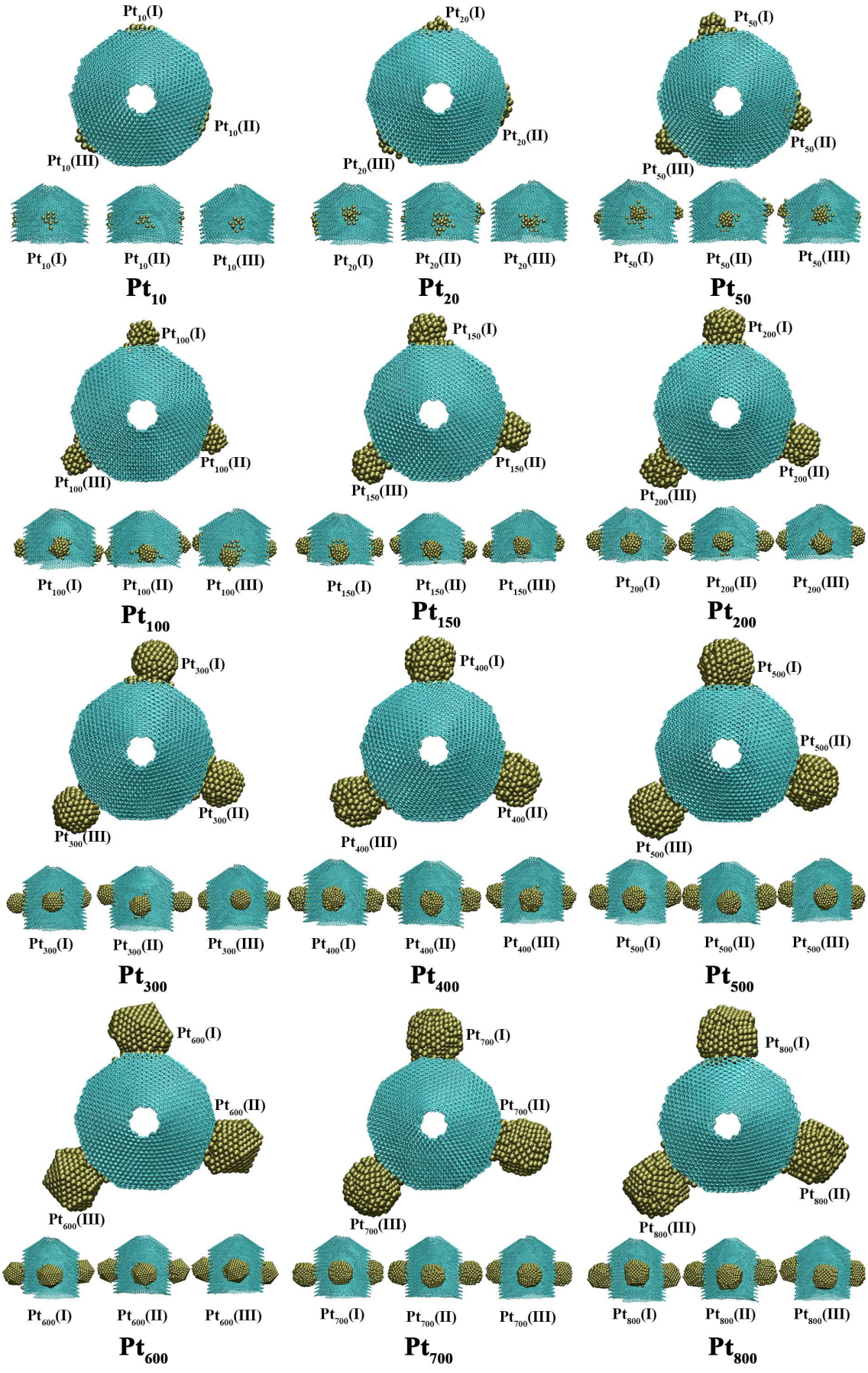
Pt10(I)
Pt10(II)
Pt10(III)
Pt10(I) Pt10(II) Pt10(III)
Pt10
Pt20(I)
Pt20(II)
Pt20(III)
Pt20(I) Pt20(II) Pt20(III)
Pt20
Pt50(I)
Pt50(II)
Pt50(III)
Pt50(I) Pt50(II) Pt50(III)
Pt50
Pt100(I)
Pt100(II)
Pt100(III)
Pt100(I) Pt100(II) Pt100(III)
Pt100
Pt150(I)
Pt150(II)
Pt150(III)
Pt150(I) Pt150(II) Pt150(III)
Pt150
Pt200(I)
Pt200(II)
Pt200(III)
Pt200(I) Pt200(II) Pt200(III)
Pt200
Pt300(I)
Pt300(II)
Pt300(III)
Pt300(I) Pt300(II) Pt300(III)
Pt300
Pt400(I)
Pt400(II)
Pt400(III)
Pt400(I) Pt400(II) Pt400(III)
Pt400
Pt500(I)
Pt500(II)
Pt500(III)
Pt500(I) Pt500(II) Pt500(III)
Pt500
Pt600(I)
Pt600(II)
Pt600(III)
Pt600(I) Pt600(II) Pt600(III)
Pt600
Pt700(I)
Pt700(II)
Pt700(III)
Pt700(I) Pt700(II) Pt700(III)
Pt700
Pt800(I)
Pt800(II)
Pt800(III)
Pt800(I) Pt800(II) Pt800(III)
Pt800

Figure 1. Schematic representations of the Pt particles adsorbed on f-CNF/60 after 250 ps of equilibrium

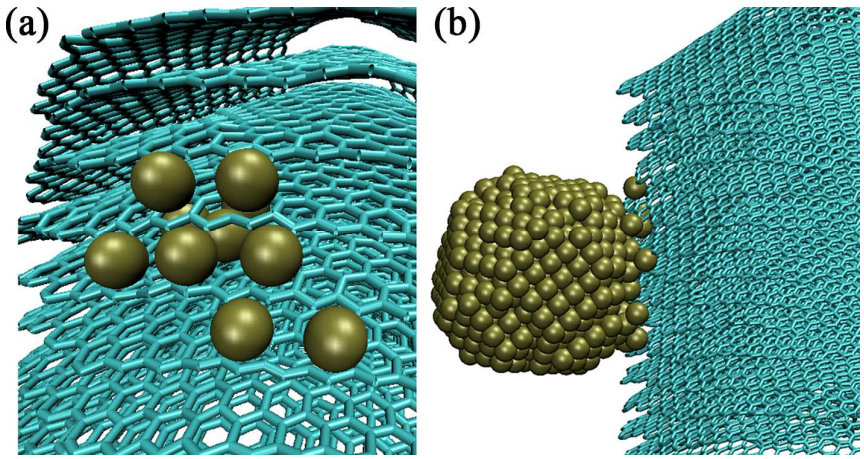

Figure 2. Schematic representations of (a) Pt_{10}(II) and (b) Pt_{800}(III) particles bonded to f-CNF/60

In order to quantitatively represent the restructuring degree of the supported Pt particles, first-shell Pt-Pt coordination number and radial distribution function are calculated and compared to those in the corresponding isolated Pt particles.

3.1.1 First-Shell Pt-Pt Coordination Number

Experimentally, it is feasible to get the mean first-shell Pt-Pt coordination number in supported metal particles, which makes it possible to compare the structural information between theoretical and experimental data. In this work, the distributions of the first-shell Pt-Pt coordination number in the Pt particles are calculated as

$$\sum_{i=0}^{12} N_i = n \qquad (1)$$

where N_i is the number of the Pt atoms that have i Pt neighbors and are counted on the basis of bond order and n is the number of atoms in the Pt particle. The data are all grouped every 500 fs, and the size of the distribution bins is 1. The statistical error is calculated as the

root-mean-square deviation in the resulting samples.

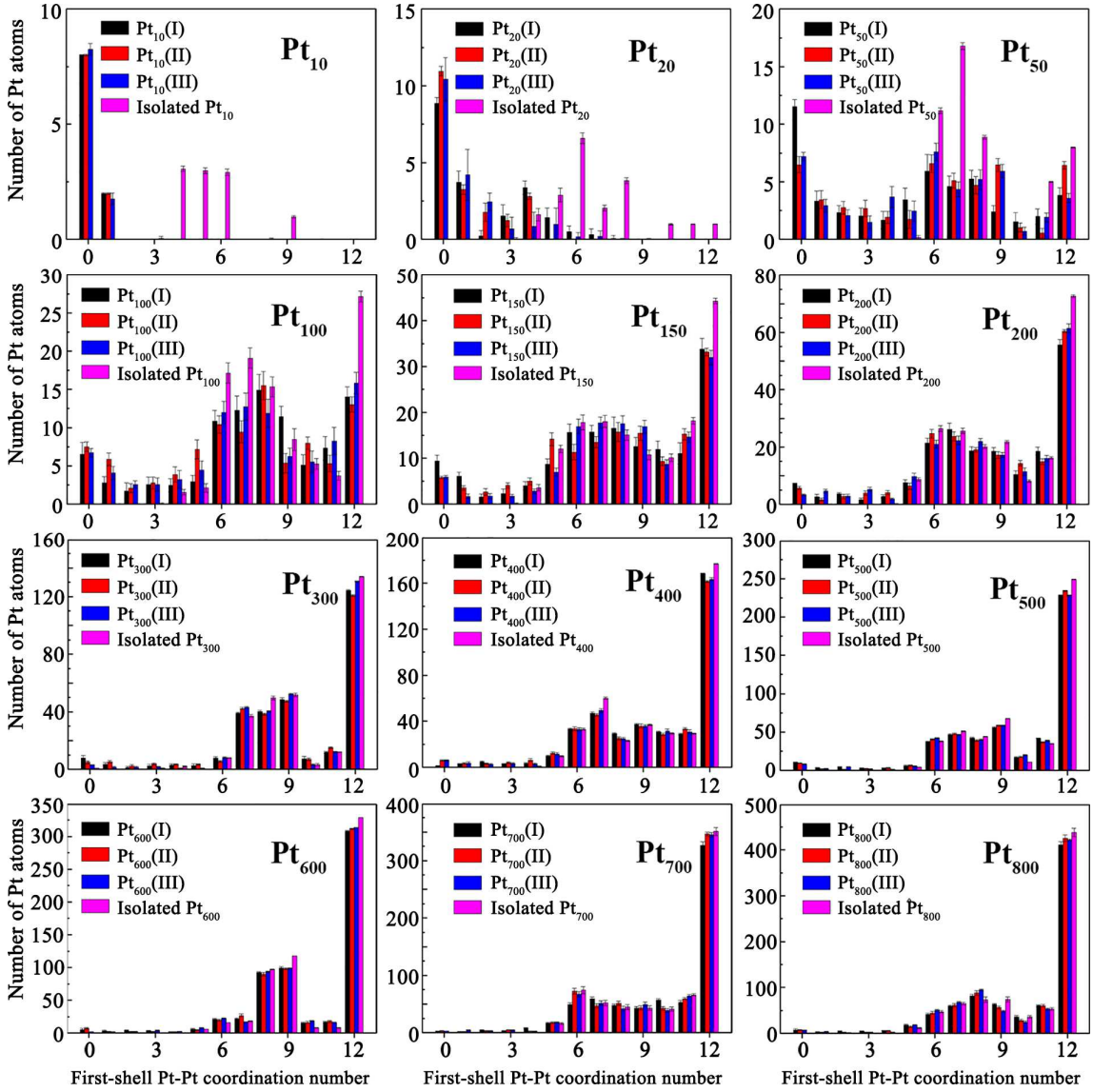

Figure 3. Comparison of first-shell Pt-Pt coordination number distributions between supported and isolated Pt particles

The distribution of the first-shell Pt-Pt coordination number varies with Pt particle size, as shown in Figure 3. In the isolated Pt particles, the first-shell Pt-Pt coordination number falls within two ranges. The Pt atoms could act as bulk atoms and have a first-shell Pt-Pt coordination number more than 10 (> 10). Alternatively, the first-shell Pt-Pt coordination number might take the value no more than 10 (≤ 10), signifying the surface nature of the Pt

atoms. In large Pt particles, the maximum probability of the first-shell Pt-Pt coordination number appears at 12 and therefore most of the bulk Pt atoms are coordinatively saturated, but in small Pt particles, the probability of first-shell Pt-Pt coordination number of 12 is zero or takes a much smaller value, indicating that all or most Pt atoms are located on the surfaces of the Pt particles. Upon adsorption the distribution of the first-shell Pt-Pt coordination number changes significantly in small Pt particles. However, when the Pt particle size is greater than 2 nm in diameter (Pt_{300}), the difference in the first-shell Pt-Pt coordination number between supported and isolated Pt particles becomes much lower. This definitely indicates particle size plays a significant role in the restructuring degree of Pt particles.

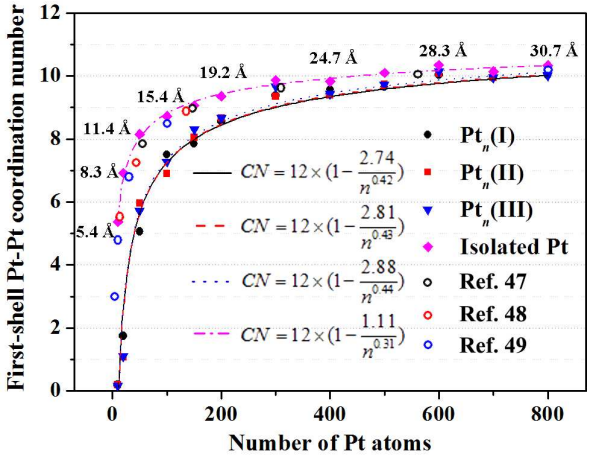

Figure 4. Relationships between the mean first-shell Pt-Pt coordination number and the number of atoms in isolated and supported Pt particles. Black, red, and blue hollow circles are adapted from refs. 47, 48, and 49, respectively.

Considering the contribution from both bulk and surface atoms, the mean first-shell Pt-Pt coordination numbers in the supported and isolated Pt particles are shown in Figure 4. Analyzing the trends in Figure 4 indicates that the relationship between the mean first-shell Pt-Pt coordination number and the number of atoms in the Pt particle can be expressed as

$$CN = a \times (1 - \frac{b}{n^c}) \quad (2)$$

where *CN* is the mean first-shell Pt-Pt coordination number in a Pt particle, *n* is the number of Pt atoms, *a* takes the value of 12, which is the first-shell coordination number in bulk Pt, and *b* and *c* are the fitted parameters, as given in Figure 4.

From Figure 4, it is apparent that the mean first-shell Pt-Pt coordination number increases with Pt particle size for both isolated and supported Pt particles, which eventually approaches the coordination number of bulk Pt atoms. In the isolated Pt particles, the mean first-shell Pt-Pt coordination number increases from 5.37 in Pt_{10} to 10.33 in Pt_{800}, as given in Table S1. In order to compare with our ReaxFF results, the mean first-shell Pt-Pt coordination numbers of different Pt particles are adapted from refs. 47, 48, and 49, respectively. Our ReaxFF results of the isolated Pt clusters are in good agreement with these reported values.

The trend in the mean first-shell Pt-Pt coordination numbers in the supported Pt particles with respect to Pt particle size is rather similar to that in the isolated Pt particles, where the coordination number is changed significantly for the Pt particles less than 2 nm in size, as shown in Figure 4. In addition, the supported Pt particle has a lower mean first-shell Pt-Pt coordination number than the isolated Pt particle of the same size, and the difference between them decreases with increasing Pt particle size; that is, upon adsorption the restructuring degree of Pt nanoparticles becomes lower as Pt particle size is increased.

3.1.2 Pt-Pt Radial Distribution Function

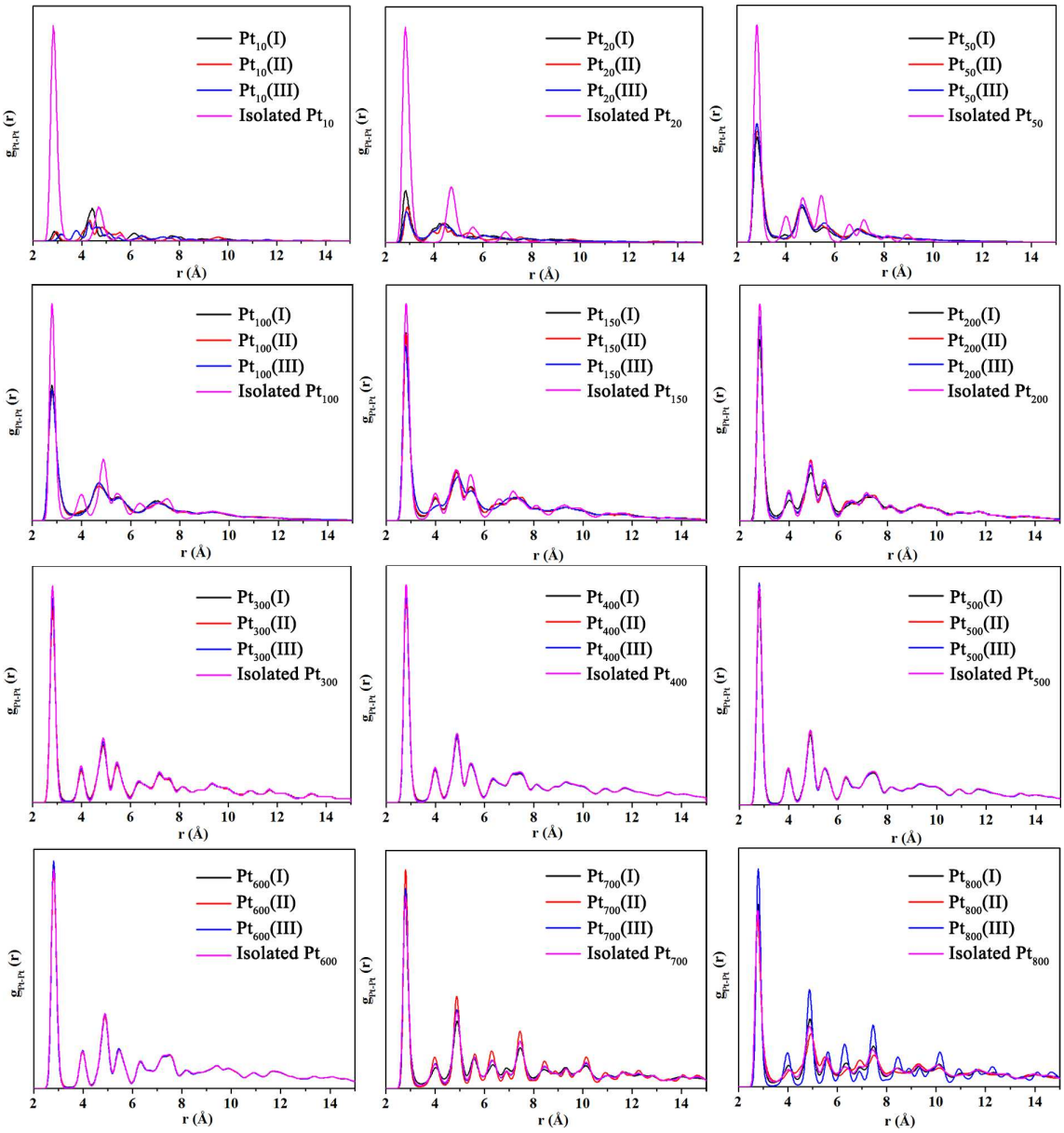

Figure 5. Pt-Pt radial distribution functions in supported and isolated Pt particles

Upon adsorption some Pt atoms migrate to the interface between Pt and f-CNF or onto the support surfaces, and therefore lattice strain is inherently introduced with particle restructuring. The degree of the lattice strain in the supported particles can be described by the comparison of Pt-Pt radial distribution function (RDF) between the supported and isolated Pt particles, as given in Figure 5. The Pt-Pt RDF, $g_{Pt\text{-}Pt}(r)$, offers a direct measure of the probability of finding another atom at a distance r from a reference Pt atom and is defined as

$$g_{Pt\text{-}Pt}(r) = \rho(r)/\overline{\rho} \quad (2)$$

where $\rho(r)$ is the density at a distance r away from a reference atom and $\overline{\rho}$ is the average density of the Pt particle.

For the isolated Pt particles the typical peak of RDF at about 2.8 Å indicates the first-shell Pt-Pt bond length. With the increase in Pt particle size, more peaks are present at longer Pt-Pt interatomic distances and become sharper. Upon adsorption the RDF in the small Pt particles is changed significantly, where the intensity of the peak present at about 2.8 Å is substantially weakened. This is induced by the significant restructuring of small Pt particles. As the particle size increases from Pt_{10} to Pt_{600}, the difference in RDF between the isolated and supported Pt particles decreases. However, what is beyond our expectation is that for Pt_{700} and Pt_{800} [e.g., Pt_{700}(II) and Pt_{800}(III)], the RDF could be even sharper than that in the isolated particles, indicating that upon adsorption the Pt particles of ~3 nm and higher in diameter have an even higher crystalline degree[50] than the corresponding isolated particles.

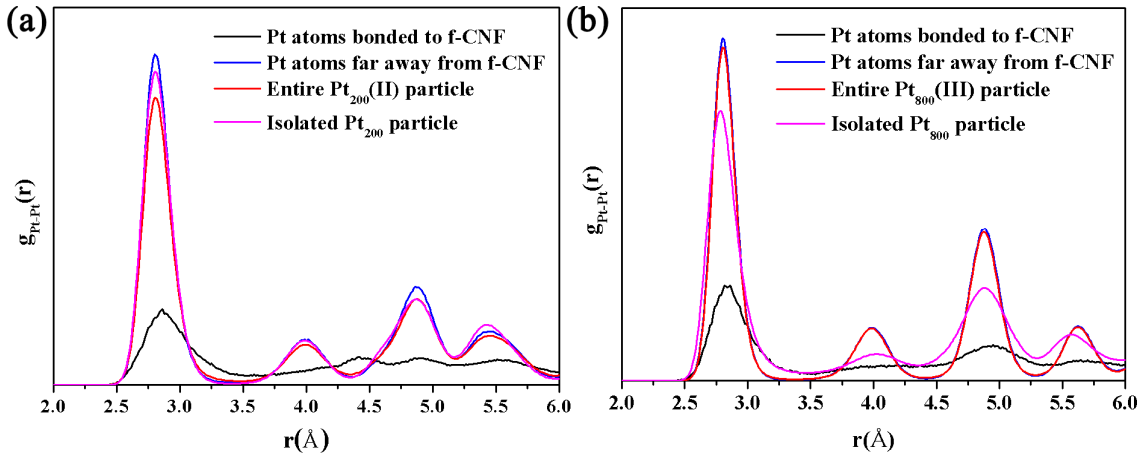

Figure 6. Pt-Pt radial distribution functions in supported (a) Pt_{200} and (b) Pt_{800}

To further elucidate the reason for this interesting phenomenon, the Pt_{200} and Pt_{800} particles are both divided into two distinct parts, namely, Pt atoms that are coordinated to f-CNF and Pt atoms that are far away from f-CNF. Under this definition, the contribution from each part of

the supported Pt particle to the overall RDF is computed, as illustrated in Figure 6. From the figure, it can be seen that for the Pt atoms that are bonded to the f-CNF, the intensity of the RDF peak present at about 2.8 Å in both Pt_{200} and Pt_{800} is weaker than that of the corresponding isolated Pt particle, indicating that the crystalline degree of the Pt atoms at the interface are lowered once Pt particles are deposited on the f-CNF support. In contrast, the RDF obtained from the Pt atoms that are far away from the f-CNF in the two Pt particles has a sharper peak at 2.8 Å than that of the corresponding isolated particle. It is rational to deduce that the increase in the crystalline degree in the upper part of the supported Pt particles arises from the strong metal-support interaction. As the RDF of the entire Pt particle is the sum of the contributions from the upper part of the particle and the Pt atoms at the Pt/f-CNF interface, the overall RDF would be affected by the ratio of these two kinds of Pt atoms. At low particle sizes, the majority of the Pt atoms is located at the interface and gives rise to a lower crystalline degree of the entire particle than that of the corresponding isolated one, while at large particle sizes the Pt atoms in the upper part of the particle are predominant, and a higher crystalline degree is attained. This provides a rational interpretation of the variation of the crystalline degree with particle size, as observed in Figure 5.

Through the comparison of the structural properties between the isolated and supported Pt particles, one can see that the restructuring degree of the Pt particles upon adsorption on f-CNF/60 decreases with the particle size. In our previous study concerning Pt_{100} particles supported on different f-CNFs, the restructuring degree of the Pt_{100} particle might vary with the surface conditions of f-CNF (i.e., the basal-to-edge surface area ratio and H termination). As only one type of f-CNFs (f-CNF/60 with a disclination angle of 60°) is used in this work to ensure that the f-CNF supports have the same surface conditions, metal particle size effect

would be responsible for the different restructuring degrees of the Pt particles upon adsorption.

3.2. Interaction between Pt Particles and f-CNF/60

3.2.1 Pt-C Bond Length Distribution

As mentioned above, the Pt particles get more closely to the f-CNF/60 surface with the formation of covalent bonds between the Pt particles and the f-CNF/60 surface. The probability distributions of Pt-C bond length are calculated to study the morphology at the interface between the Pt particles and f-CNF/60, as shown in Figure 7. The probability distributions of the bond lengths are normalized in the range $[x_1, x_2]$ in such a way that

$$\int_{x_1}^{x_2} P(x)\mathrm{d}x = 1 \tag{3}$$

where x_1 = 1.8 Å and x_2 = 2.8 Å for the Pt-C bonds to ensure that only Pt atoms bonded to carbon atoms are taken into account. The atomic coordinates are recorded every 25 fs. The data are all grouped every 500 fs and the statistical error is calculated as the root-mean-square deviation in the resulting samples. The size of the distribution bins is taken as small as 0.0125 Å to get a smooth curve, and the average error bars are given every five points to obtain a clear plot.

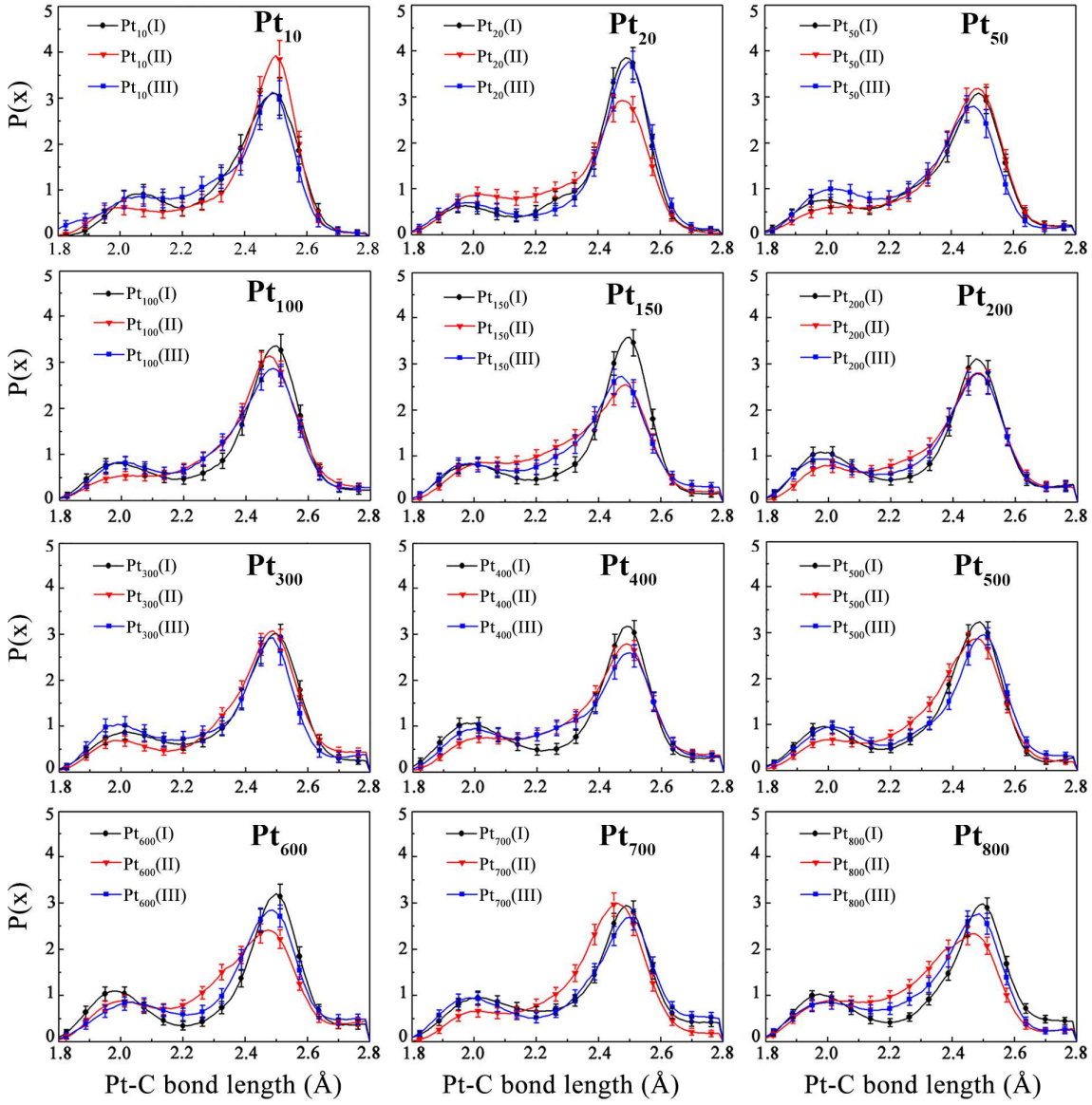

Figure 7. Probability densities of Pt-C bond length distributions at the interface between Pt particles and f-CNF/60

From Figure 7, it can be seen that for all the Pt-CNF systems two pronounced peaks are observed at the Pt-C bond lengths of about 2.0 and 2.5 Å, which are quite close to those in Pt_{100} particles deposited on different f-CNFs[26] and also compare closely to experimentally obtained EXAFS data.[51,52] Moreover, the majority of the Pt particles supported on f-CNF/60 have similar Pt-C bond length distribution (i.e., close molar ratio of the probability of long to short Pt-C bonds), except that for some small Pt particles including Pt_{10}(II), Pt_{20}(I), and Pt_{20}(III), the

probability of the Pt-C bond length of 2.5 Å is higher. In our previous study of Pt_{100} adsorbed on f-CNF,[26] the Pt-C bond length distribution of Pt_{100} particle varies with the basal-to-edge surface area ratio and also depends on whether the f-CNF is terminated by H, which is eventually determined by how frequently Pt atoms are in contact with the edge (or basal) planes. On the basis of this information, it can be deduced the similar Pt-C bond length distribution observed in this work arises from the same superficial structure of the f-CNF/60 support, while the different metal particle sizes adopted have a minor effect. In Pt_{10}(II), Pt_{20}(I), and Pt_{20}(III), a few Pt atoms move into the interlayer between two adjacent graphene sheets and interact only with the basal planes, as illustrated in Figure 2a, thereby leading to an increase in the probability of the Pt-C bond length of 2.5 Å.

3.2.2 Binding Strength of Pt Particles to f-CNF/60

To quantitatively represent the Pt-CNF interaction, the binding energy of the Pt particles to f-CNF/60 is defined as

$$E_b = E_{\text{Pt/f-CNF}} - E_{\text{Pt}} - E_{\text{f-CNF}} \quad (4)$$

where $E_{\text{Pt/f-CNF}}$ is the average total energy of the Pt particle adsorbed on the f-CNF upon 250 ps of equilibrium, E_{Pt} is the average total energy of the isolated Pt particle with the fixed geometry upon adsorption, and $E_{\text{f-CNF}}$ is the average total energy of the f-CNF. Under this definition, a more negative binding energy indicates a stronger binding strength between the Pt particles and the f-CNF. The relationship between the binding energies of the Pt particles and the number of the Pt atoms bonded to f-CNFs is shown in Figure 8.

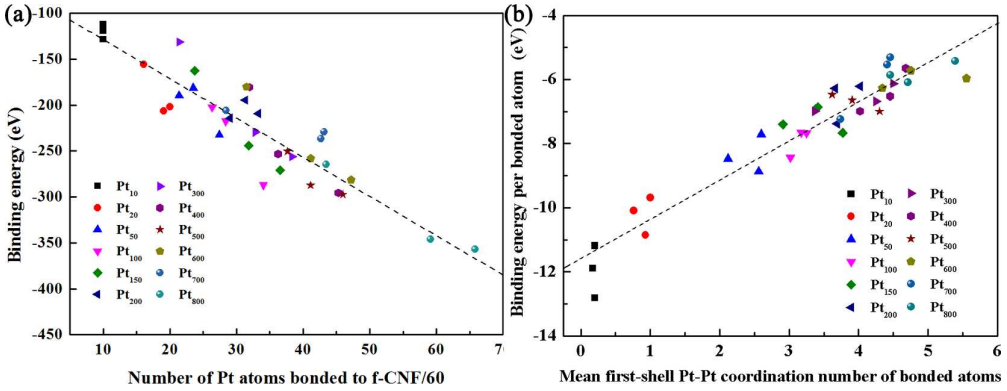

Figure 8. (a) Relationship between the binding energies of the Pt particles and the number of Pt atoms bonded to f-CNF/60; (b) Relationship between the binding energy per bonded atom and the mean first-shell Pt-Pt coordination number of the Pt atom bonded to f-CNF/60

A reference line (the dashed line in Figure 8a) is fitted to show the dependence of the binding energy of Pt particles on the number of Pt atoms bonded to f-CNF/60. It is apparent that with the increase in the number of Pt atoms bonded to the f-CNF/60 surfaces, a greater binding strength is obtained. Carefully analyzing the relationship between the binding energy and the number of Pt atoms bonded to f-CNF/60, we found that for a given number of Pt atoms bonded to f-CNF/60 the binding strength of small Pt particles is greater than that of large Pt particles; that is, the binding energy per bonded atom in small Pt particles is more negative than that in large Pt particles. In small Pt particles most bonded atoms are single Pt adatoms which interact only with the f-CNF, but in large Pt particles the bonded Pt atom interacts not only with f-CNF but also with other Pt atoms (i.e., having a higher Pt-Pt coordination number). The relationship between the binding energy per bonded atoms and the mean first-shell Pt-Pt coordination number of the bonded atoms is shown in Figure 8b. One can see the binding strength per Pt atom bonded to f-CNF/60 decreases with the increase in the mean first-shell Pt-Pt coordination number of the bonded atoms. In large Pt particles, the Pt atom bonded to f-CNF/60 has a higher mean first-shell Pt-Pt coordination number and thus lower binding strength per bonded atom

than that in small Pt particles. In early DFT calculations of Pt particles adsorption on graphene,[53] the interaction energy of two single Pt atoms with graphene is greater than that of a Pt dimer, which supports our conclusion that a higher Pt-Pt coordination number of bonded atoms leads to a less negative binding energy per bonded atom.

In our previous study concerning Pt_{100} particles adsorbed on f-CNFs, greater interaction strength between Pt particles and f-CNF gives rise to a higher restructuring degree of Pt_{100} particle.[26] In the present work, large Pt particles inherently have larger contact region and thus more Pt atoms bonded to f-CNF than small ones, leading to a stronger interaction with f-CNF/60. However, a lower restructuring degree is simultaneously observed, as evidenced by the aforementioned comparison of first shell Pt-Pt coordination number and radial distribution function between isolated and supported Pt particles. Thus, the restructuring degree of the Pt particles cannot be quantified simply by the interaction strength, once Pt particles of different sizes are taken into account. On the contrary, the binding energy per bonded Pt atom offers a measure of how strongly Pt atoms tend to move from metal particles to the Pt/f-CNF interface or support surfaces. With the increase in Pt particle size, the driving force for the formation of single Pt sites is lowered.

3.3 Cohesive Energy of Pt Particle

Apart from the binding energy per bonded Pt atom, the cohesive energy of Pt particles could probably have an effect on the restructuring of metal particles. The cohesive energy of Pt particles is plotted against metal particle size, as shown in Figure 9. Analyzing the relationship between them, we found that the cohesive energy of Pt particles can be expressed as

$$E_{\text{cohesive}} = 5.79 \times (1 - \frac{0.73}{\sqrt[3]{n}}) \quad (5)$$

where E_{cohesive} is the cohesive energy of a Pt particle, n is the number of atoms comprising the Pt particle, and 5.79 (eV) is the cohesive energy of bulk Pt calculated through ReaxFF, which is close to the experimental value of 5.84 eV.[54]

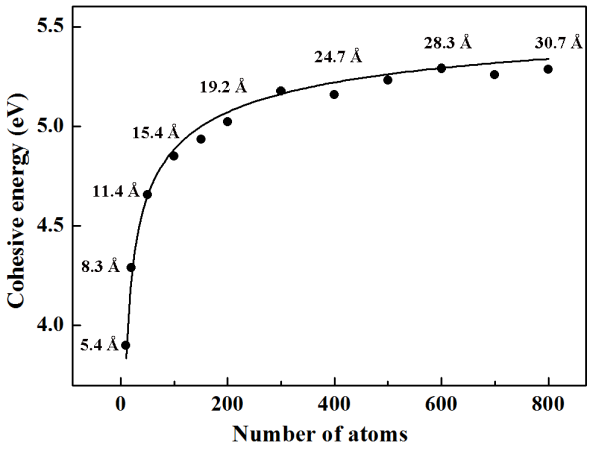

Figure 9. Relationship between cohesive energy and Pt particle size

From Figure 9 and Eq. 5, one can see that the cohesive energy of the Pt particles increases with Pt particle size, which is in good agreement with the results of the isolated Pt particles reported by Qi and Wang.[55] The decrease in the cohesive energy of the supported Pt particles implies the decrease in the number of Pt-Pt bonds per atom and in the strength of Pt-Pt bonds. Therefore, in small Pt particles Pt-Pt bonds can be readily broken, leading to the migration of Pt atoms from Pt particles to f-CNF surfaces. As a consequence, the ratio of the bonded to overall Pt atoms increases and a more significant restructuring of Pt particles results. On the other hand, the majority of the Pt atoms in large Pt particles is located far from the f-CNF surface and the high cohesive energy makes Pt atoms difficult to migrate from metal particles to f-CNF, giving rise to a less restructuring degree.

It should be noted that in small Pt particles, especially in the Pt_{10} particle, the majority of the Pt atoms is detached from the particle, leading to atomic adsorption of single Pt atoms on the f-CNF/60. It was reported that the catalyst with single Pt atoms supported on the surfaces of

iron oxide has maximum efficiency and shows excellent stability and high activity for both CO oxidation and preferential oxidation of CO in H_2.[56] According to our findings, it is essential to lower the size of the Pt particles deposited on f-CNFs during catalyst preparation, in order to strengthen the Pt-CNF interaction and to attain a lower cohesive energy of metal particles, which eventually gives rise to single Pt atoms adsorbed on supports.

3.4 Surface Properties of Supported Pt Particles

3.4.1 Pt Dispersion

As the active metal surfaces play a vital role in heterogeneous catalysis, and because the restructuring degree of Pt particles upon adsorption varies with particle size, we move on to examine the effect of particle size on the surface properties of the supported Pt particles. Metal dispersion which is defined as the molar ratio of surface to overall metal atoms in particles,[49] is an important property that can be experimentally measured by CO or H_2 adsorption, or TEM. A higher dispersion implies more atoms exposed and a higher catalytic efficiency for structure-insensitive reactions.

The location of Pt atoms in particles is identified by first-shell Pt-Pt coordination number. A Pt atom with a first-shell coordination number of 12 signifies its bulk nature and a lower coordination number indicates that it is located on the surface.[57] In the isolated nanoparticles, Pt atoms are coordinated solely to the other Pt atoms, while in the supported particles Pt atoms could be bonded either to Pt or to C atoms. Consequently, for all the Pt atoms in the isolated Pt particles and the majority of Pt atoms in the supported Pt particle which are not bonded to the f-CNF/60, the surface atom is identified by the first-shell Pt-Pt coordination number being no more than 10, as proposed by Lee et al.[57] For the Pt atoms bonded to the f-CNF/60, the surface atom is identified by the first-shell Pt-Pt coordination number being no more than 4.

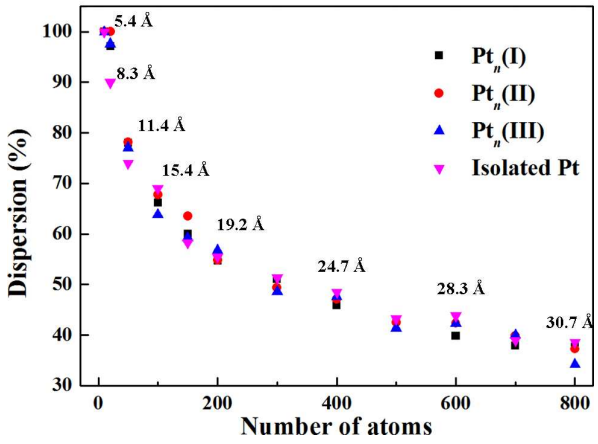

Figure 10. Relationship between the Pt dispersion and the number of atoms involved in isolated and supported Pt particles

The relationship between Pt dispersion and the number of atoms involved in isolated and supported particles is given in Figure 10. From the figure, it can be seen that the supported metal particles have rather a close Pt dispersion to the isolated metal particles of the same size. A variety of surface sites of Pt particle are inherently eliminated upon adsorption. Nevertheless, for small Pt particles, adsorption-induced restructuring tends to raise the dispersion of the supported particles to be comparable to that of the particles in vacuum, while for large Pt particles, the ratio of eliminated to overall surfaces is rather low, giving rise to a close Pt dispersion of the supported metal particles to those of isolated ones. With the increase in Pt particle size, Pt dispersion of the isolated and supported Pt particles decreases.

3.4.2 Coordination Number of Surface Atoms on Pt Particles.

Metal particle size (and hence the coordination number of surface atoms) plays a significant role in structure-sensitive reactions. For instance, in the ORR the oxygenated species acting as reaction intermediates have stronger binding strength to small Pt particles, and the energy barrier for water formation at the coordinately unsaturated sites was found to be considerably

increased.[20]

The relationship between the mean first-shell Pt-Pt coordination number of surface Pt atoms and the particle size is shown in Figure 11 (more details are given in Table S2). Through the comparison between Figures 4 and 11, one can see that the surface Pt atoms have a lower mean first-shell Pt-Pt coordination number than the overall Pt atoms in both the isolated and the supported particles, and the trend in the mean first-shell Pt-Pt coordination number of the surface Pt atoms with respect to the particle size is similar to that of the overall Pt atoms, i.e., the mean first-shell Pt-Pt coordination number of surface Pt atoms increases with the particle size. The relationship between the mean first-shell Pt-Pt coordination number of surface atoms and the number of atoms in Pt particle can also be represented by Eq. 2. With the increase in Pt particle size the mean first-shell Pt-Pt coordination number of surface atoms gradually approach that of the Pt atoms on the close-packed facet, and therefore the parameter *a* takes the value of 9 and the fitted parameters are shown in Figure 11. The mean first-shell Pt-Pt coordination number of surface Pt atom increases with the Pt particle size. According to the *d*-band model[58], a lower coordination number of late transition metal atoms gives rise to a narrower *d*-band and thus an upshift of *d*-band center in energy, which usually causes a stronger chemisorption at these sites. Therefore, for structure-sensitive reactions it raises the possibility of tailoring the catalytic behavior of metal particle by controlling the particle size.

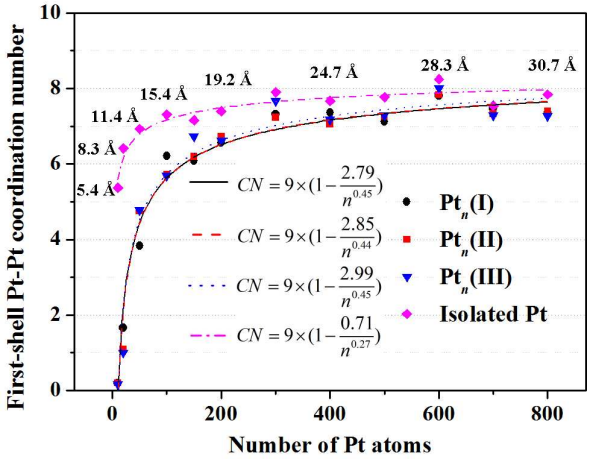

Figure 11. Relationships between the mean first-shell Pt-Pt coordination number of surface Pt atoms and the number of atoms in isolated and supported Pt particles

4. CONCLUSION

MD simulations based on the ReaxFF have been performed to examine the structural evolution of f-CNF/60-supported Pt particles of different sizes. Twelve Pt particles with the number of atoms ranging from 10 to 800 are employed, with the Pt particle size in the range of 5.6-30.7 Å. Calculated results indicate upon adsorption the distribution of the first-shell Pt-Pt coordination number and radial distribution function change significantly in small Pt particles that have diameters less than 2 nm. When the Pt particle size is greater than 2 nm (Pt_{300}), the restructuring degree of the supported Pt particles becomes much lower. As the Pt particle size is increased to ~3 nm (Pt_{700} and Pt_{800}), however, the crystalline degree of Pt nanoparticles is even higher than that of the corresponding isolated ones because the strong metal-support interaction has a positive effect on the crystalline degree of the upper part of Pt nanoparticles. This definitely indicates particle size plays a significant role in the restructuring of Pt particles.

Upon adsorption Pt-C bonds are formed at the interface between the Pt particles and the f-CNF/60, and the Pt-C bond distribution depends strongly on the surface conditions of the f-CNF while the variation in particle size has a minor effect. As the Pt particle size increases,

the binding energy per Pt atom bonded to f-CNF becomes less negative and results in a weaker interaction between the Pt atoms and the f-CNF/60. On the other hand, small Pt particles have a lower cohesive energy and the Pt-Pt bond can be readily broken, leading to the migration of Pt atoms from Pt particles to f-CNF surfaces. Therefore, in order to prepare catalyst with single Pt atoms, it is essential to lower the size of the Pt particles deposited on f-CNFs during catalyst preparation. In contrast, the majority of the Pt atoms in large Pt particles are located far from the f-CNF surface and the high cohesive energy makes Pt atoms difficult to be detached from metal particles to f-CNF. Therefore, both the reduced binding energy per bonded Pt atom and the increased cohesive energy are responsible for the less restructuring degree.

With the increase in particle size, two surface properties of the Pt particles, namely, Pt dispersion and surface first-shell Pt-Pt coordination number are found to decrease and increase, respectively. For structure-sensitive reaction, these findings raise the possibility of tailoring the catalytic behavior of metal particles by controlling particle size.

ACKNOWLEDGMENTS

This work is supported by 863 Program of Ministry of Science and Technology of China (No. 2012AA040306), Natural Science Foundation of China (No. 21276077, 21406063, and 21473053) and China Postdoctoral Science Foundation (2014M551346). The computational time provided by the Notur project is highly acknowledged.

Supporting Information

Videos of the evolution of supported Pt particles, Mean first-shell Pt-Pt coordination number of overall and surface atoms in both isolated and supported Pt particles. This information is available free of charge via the Internet at http://pubs.acs.org

REFERENCES

(1) Norskov, J. K.; Bligaard, T.; Hvolbaek, B.; Abild-Pedersen, F.; Chorkendorff, I.; Christensen, C. H. The nature of the active site in heterogeneous metal catalysis. *Chem. Soc. Rev.* **2008**, *37*, 2163-2171.

(2) Arenz, M.; Mayrhofer, K. J. J.; Stamenkovic, V.; Blizanac, B. B.; Tomoyuki, T.; Ross, P. N.; Markovic, N. M. The effect of the particle size on the kinetics of CO electrooxidation on high surface area Pt catalysts. *J. Am. Chem. Soc.* **2005**, *127*, 6819-6829.

(3) Frelink, T.; Visscher, W.; Van Veen, J. Particle size effect of carbon-supported platinum catalysts for the electrooxidation of methanol. *J. Electroanal. Chem.* **1995**, *382*, 65-72.

(4) Shao, M. H.; Peles, A.; Shoemaker, K. Electrocatalysis on Platinum Nanoparticles: Particle Size Effect on Oxygen Reduction Reaction Activity. *Nano Lett.* **2011**, *11*, 3714-3719.

(5) Kumar, M. S.; Chen, D.; Walmsley, J. C.; Holmen, A. Dehydrogenation of propane over Pt-SBA-15: Effect of Pt particle size. *Catal. Commun.* **2008**, *9*, 747-750.

(6) Yang, M. L.; Zhu, Y. A.; Fan, C.; Sui, Z. J.; Chen, D.; Zhou, X. G. DFT study of propane dehydrogenation on Pt catalyst: effects of step sites. *Phys. Chem. Chem. Phys.* **2011**, *13*, 3257-3267.

(7) Boudart, M.; Djega-Mariadassou, G. *Kinetics of Heterogeneous Catalytic Reactions*; Princeton University Press: Princeton, 1984.

(8) Somorjai, G. A. *Introduction to Surface Chemistry and Catalysis*; Wiley-Interscience: New York, 1994.

(9) Lin, Y. H.; Cui, X. L.; Yen, C.; Wai, C. M. Platinum/carbon nanotube nanocomposite synthesized in supercritical fluid as electrocatalysts for low-temperature fuel cells. *J. Phys. Chem. B* **2005**, *109*, 14410-14415.

(10) Costamagna, P.; Srinivasan, S. Quantum Jumps in the PEMFC Science and Technology from the 1960s to the Year 2000 Part I. Fundamental Scientific Aspects. *J. Power Sources* **2001**, *102*, 242-252.

(11) Jayaraman, S.; Hillier, A. C. Electrochemical Synthesis and Reactivity Screening of a Ternary Composition Gradient for Combinatorial Discovery of Fuel Cell Catalysts. *Meas. Sci. Technol.* **2005**, *16*, 5-13.

(12) Takasu, Y.; Iwazaki, T.; Sugimoto, W.; Murakami, Y. Size effects of platinum particles on the electro-oxidation of methanol in an aqueous solution of HClO4. *Electrochem. Commun.* **2000**, *2*, 671-674.

(13) Park, S.; Xie, Y.; Weaver, M. J. Electrocatalytic Pathways on Carbon-Supported Platinum Nanoparticles: Comparison of Particle-Size-Dependent Rates of Methanol, Formic Acid, and Formaldehyde Electrooxidation. *Langmuir* **2002**, *18*, 5792-5798.

(14) Kinoshita, K. Particle size effects for oxygen reduction on highly dispersed platinum in acid electrolytes. *J. Electrochem. Soc.* **1990**, *137*, 845-848.

(15) Mukerjee, S. Particle size and structural effects in platinum electrocatalysis. *J. Appl. Electrochem.* **1990**, *20*, 537-548.

(16) Gasteiger, H. A.; Kocha, S. S.; Sompalli, B.; Wagner, F. T. Activity benchmarks and requirements for Pt, Pt-alloy, and non-Pt oxygen reduction catalysts for PEMFCs. *Appl Catal B-Environ* **2005**, *56*, 9-35.

(17) Stephens, I. E. L.; Bondarenko, A. S.; Gronbjerg, U.; Rossmeisl, J.; Chorkendorff, I. Understanding the electrocatalysis of oxygen reduction on platinum and its alloys. *Energ Environ Sci* **2012**, *5*, 6744-6762.

(18) Mayrhofer, K. J. J.; Blizanac, B. B.; Arenz, M.; Stamenkovic, V. R.; Ross, P. N.; Markovic, N. M. The Impact of Geometric and Surface Electronic Properties of Pt-Catalysts on the Particle Size Effect in Electrocatalysis. *The Journal of Physical Chemistry B* **2005**, *109*, 14433-14440.

(19) Mayrhofer, K. J. J.; Strmcnik, D.; Blizanac, B. B.; Stamenkovic, V.; Arenz, M.; Markovic, N. M. Measurement of oxygen reduction activities via the rotating disc electrode method: From Pt model surfaces to carbon-supported high surface area catalysts. *Electrochim. Acta* **2008**, *53*, 3181-3188.

(20) Greeley, J.; Rossmeisl, J.; Hellman, A.; Norskov, J. K. Theoretical trends in particle size effects for the oxygen reduction reaction. *Z Phys Chem* **2007**, *221*, 1209-1220.

(21) Tritsaris, G. A.; Greeley, J.; Rossmeisl, J.; Norskov, J. K. Atomic-Scale Modeling of Particle Size Effects for the Oxygen Reduction Reaction on Pt. *Catal. Lett.* **2011**, *141*, 909-913.

(22) Stiles, A. B. *Catalyst Supports and Supported Catalysts*; Butterworth Publishers, Stoneham, MA: United States, 1987.

(23) Melechko, A. V.; Merkulov, V. I.; McKnight, T. E.; Guillorn, M. A.; Klein, K. L.; Lowndes, D. H.; Simpson, M. L. Vertically Aligned Carbon Nanofibers and Related Structures: Controlled Synthesis and Directed Assembly. *J. Appl. Phys.* **2005**, *97*, 041301-041339.

(24) Antolini, E. Carbon Supports for Low-Temperature Fuel Cell Catalysts. *Appl. Catal., B* **2009**, *88*, 1-24.

(25) Bessel, C. A.; Laubernds, K.; Rodriguez, N. M.; Baker, R. T. K. Graphite Nanofibers as an Electrode for Fuel Cell Applications. *J. Phys. Chem. B* **2001**, *105*, 1115-1118.

(26) Cheng, H. Y.; Zhu, Y. A.; Astrand, P. O.; Chen, D.; Li, P.; Zhou, X. G. Evolution of Pt Nanoparticles Supported on Fishbone-Type Carbon Nanofibers with Cone-Helix Structures: A Molecular Dynamics Study. *J. Phys. Chem. C* **2013**, *117*, 14261-14271.

(27) Tersoff, J. New empirical approach for the structure and energy of covalent systems. *Phys. Rev. B* **1988**, *37*, 6991-7000.

(28) Brenner, D. W. Empirical Potential for Hydrocarbons for Use in Simulating the Chemical Vapor-Deposition of Diamond Films. *Phys. Rev. B* **1990**, *42*, 9458-9471.

(29) Rappe, A. K.; Goddard, W. A. Charge Equilibration for Molecular-Dynamics Simulations. *J. Phys. Chem.* **1991**, *95*, 3358-3363.

(30) van Duin, A. C. T.; Dasgupta, S.; Lorant, F.; Goddard, W. A. ReaxFF: A Reactive Force Field for Hydrocarbons. *J. Phys. Chem. A* **2001**, *105*, 9396-9409.

(31) Nielson, K. D.; van Duin, A. C. T.; Oxgaard, J.; Deng, W. Q.; Goddard, W. A. Development of the ReaxFF Reactive Force Field for Describing Transition Metal Catalyzed Reactions, with Application to the Initial Stages of the Catalytic Formation of Carbon Nanotubes. *J. Phys. Chem. A* **2005**, *109*, 493-499.

(32) van Duin, A. C. T.; Strachan, A.; Stewman, S.; Zhang, Q. S.; Xu, X.; Goddard, W. A. ReaxFF(SiO) Reactive Force Field for Silicon and Silicon Oxide Systems. *J. Phys. Chem. A* **2003**, *107*, 3803-3811.

(33) Zhang, Q.; Cagin, T.; van Duin, A. C. T.; Goddard, W. A.; Qi, Y.; Hector, L. G. Adhesion and Nonwetting-Wetting Transition in the Al/α-Al_2O_3 Interface. *Phys. Rev. B* **2004**, *69*, 045423.

(34) Cheung, S.; Deng, W. Q.; van Duin, A. C. T.; Goddard, W. A. ReaxFF(MgH) Reactive Force Field for Magnesium Hydride Systems. *J. Phys. Chem. A* **2005**, *109*, 851-859.

(35) Han, S. S.; van Duin, A. C. T.; Goddard, W. A.; Lee, H. M. Optimization and Application of Lithium Parameters for the Reactive Force Field, ReaxFF. *J. Phys. Chem. A* **2005**, *109*, 4575-4582.

(36) Goddard, W. A.; van Duin, A. C. T.; Chenoweth, K.; Cheng, M. J.; Pudar, S.; Oxgaard, J.; Merinov, B.; Jang, Y. H.; Persson, P. Development of the ReaxFF Reactive Force Field for Mechanistic Studies of Catalytic Selective Oxidation Processes on BiMoOx. *Top. Catal.* **2006**, *38*, 93-103.

(37) Jarvi, T. T.; van Duin, A. C. T.; Nordlund, K.; Goddard, W. A. Development of Interatomic ReaxFF Potentials for Au-S-C-H Systems. *J. Phys. Chem. A* **2011**, *115*, 10315-10322.

(38) Neyts, E. C.; Shibuta, Y.; van Duin, A. C. T.; Bogaerts, A. Catalyzed Growth of Carbon Nanotube with Definable Chirality by Hybrid Molecular Dynamics-Force Biased Monte Carlo Simulations. *Acs Nano* **2010**, *4*, 6665-6672.

(39) Neyts, E. C.; van Duin, A. C. T.; Bogaerts, A. Changing Chirality during Single-Walled Carbon Nanotube Growth: A Reactive Molecular Dynamics/Monte Carlo Study. *J. Am. Chem. Soc.* **2011**, *133*, 17225-17231.

(40) Pigos, E.; Penev, E. S.; Ribas, M. A.; Sharma, R.; Yakobson, B. I.; Harutyunyan, A. R. Carbon Nanotube Nucleation Driven by Catalyst Morphology Dynamics. *Acs Nano* **2011**, *5*, 10096-10101.

(41) Sanz-Navarro, C. F.; Astrand, P. O.; Chen, D.; Ronning, M.; van Duin, A. C. T.; Jacob, T.; Goddard, W. A. Molecular Dynamics Simulations of the Interactions between Platinum Clusters and Carbon Platelets. *J. Phys. Chem. A* **2008**, *112*, 1392-1402.

(42) Sanz-Navarro, C. F.; Astrand, P. O.; Chen, D.; Ronning, M.; van Duin, A. C. T.; Goddard, W. A. Molecular Dynamics Simulations of Metal Clusters Supported on Fishbone Carbon Nanofibers. *J. Phys. Chem. C* **2010**, *114*, 3522-3530.

(43) LAMMPS WWW Site.

(44) Plimpton, S. Fast Parallel Algorithms for Short-Range Molecular Dynamics. *J. Comput. Phys.* **1995**, *117*, 1-19.

(45) Martyna, G. J.; Klein, M. L.; Tuckerman, M. Nose-Hoover Chains: The Canonical Ensemble Via Continuous Dynamics. *J. Chem. Phys.* **1992**, *97*, 2635-2643.

(46) Cheng, H. Y.; Zhu, Y. A.; Sui, Z. J.; Zhou, X. G.; Chen, D. Modeling of Fishbone-Type Carbon Nanofibers with Cone-Helix Structures. *Carbon* **2012**, *50*, 4359-4372.

(47) Beale, A. M.; Weckhuysen, B. M. EXAFS as a tool to interrogate the size and shape of mono and bimetallic catalyst nanoparticles. *Phys. Chem. Chem. Phys.* **2010**, *12*, 5562-5574.

(48) de Graaf, J.; van Dillen, A. J.; de Jong, K. P.; Koningsberger, D. C. Preparation of highly dispersed Pt particles in zeolite Y with a narrow particle size distribution: Characterization by hydrogen chemisorption, TEM, EXAFS spectroscopy, and particle modeling. *J. Catal.* **2001**, *203*, 307-321.

(49) Kip, B. J.; Duivenvoorden, F. B. M.; Koningsberger, D. C.; Prins, R. Determination of Metal-Particle Size of Highly Dispersed Rh, Ir, and Pt Catalysts by Hydrogen Chemisorption and EXAFS. *J. Catal.* **1987**, *105*, 26-38.

(50) Kazanc, S. Molecular dynamics study of pressure effect on glass formation and the crystallization in liquid CuNi alloy. *Comp Mater Sci* **2006**, *38*, 405-409.

(51) Zhang, Y. H.; Toebes, M. L.; van der Eerden, A.; O'Grady, W. E.; de Jong, K. P.; Koningsberger, D. C. Metal Particle Size and Structure of the Metal-Support Interface of Carbon-Supported Platinum Catalysts as Determined with EXAFS Spectroscopy. *J. Phys. Chem. B* **2004**, *108*, 18509-18519.

(52) Toebes, M. L.; Zhang, Y. H.; Hajek, J.; Nijhuis, T. A.; Bitter, J. H.; van Dillen, A. J.; Murzin, D. Y.; Koningsberger, D. C.; de Jong, K. P. Support Effects in the Hydrogenation of Cinnamaldehyde over Carbon Nanofiber-Supported Platinum Catalysts: Characterization and Catalysis. *J. Catal.* **2004**, *226*, 215-225.

(53) Okazaki-Maeda, K.; Morikawa, Y.; Tanaka, S.; Kohyama, M. Structures of Pt Clusters on Graphene by First-Principles Calculations. *Surf. Sci.* **2010**, *604*, 144-154.

(54) Kittel, C. *Introduction to Solid State Physics*; John Wiley & Sons: New York, 1996.

(55) Qi, W. H.; Wang, M. P. Size effect on the cohesive energy of nanoparticle. *J. Mater. Sci. Lett.* **2002**, *21*, 1743-1745.

(56) Qiao, B. T.; Wang, A. Q.; Yang, X. F.; Allard, L. F.; Jiang, Z.; Cui, Y. T.; Liu, J. Y.; Li, J.; Zhang, T. Single-atom catalysis of CO oxidation using Pt-1/FeOx. *Nat. Chem.* **2011**, *3*, 634-641.

(57) Lee, Y. J.; Lee, E. K.; Kim, S.; Nieminen, R. M. Effect of Potential Energy Distribution on the Melting of Clusters. *Phys. Rev. Lett.* **2001**, *86*, 999-1002.

(58) Hammer, B.; Norskov, J. K. Theoretical Surface Science and Catalysis - Calculations and Concepts. *Adv. Catal.* **2000**, *45*, 71-129.

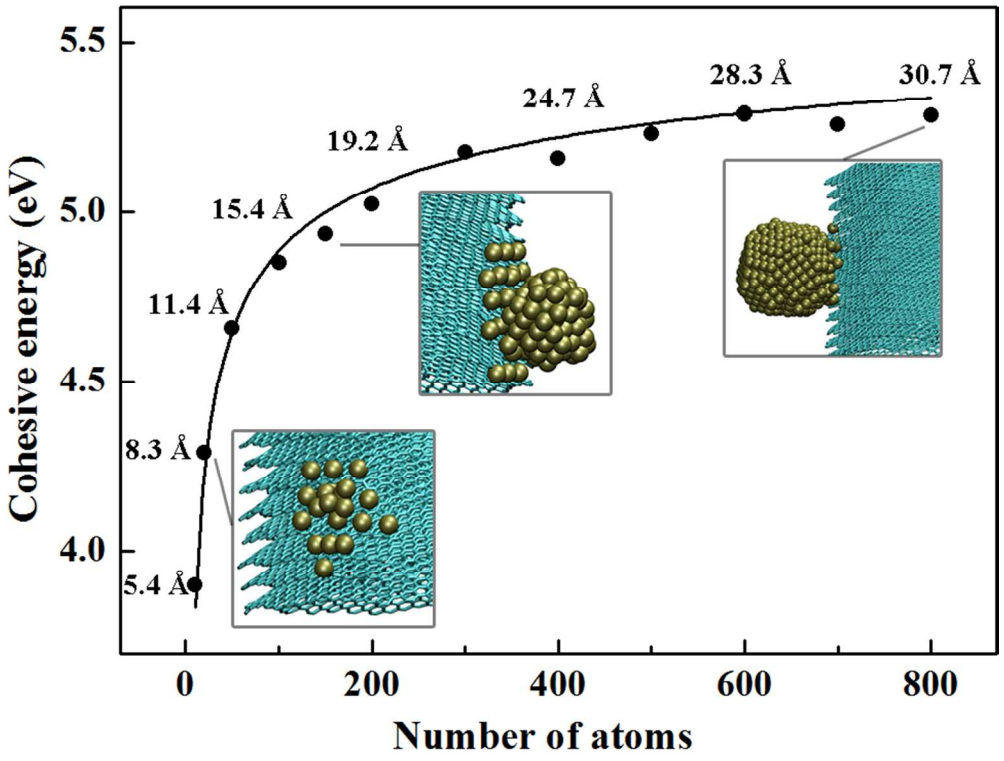

82x62mm (300 x 300 DPI)